

ELECTROMAGNETIC COUPLING IN FREQUENCY AND TIME-DOMAIN INDUCED-POLARIZATION SURVEYS OVER A MULTILAYERED EARTH†

ABHIJIT DEY* AND H. FRANK MORRISON*

Electromagnetic coupling responses in frequency and time-domain induced-polarization measurements over a multilayered earth are evaluated. For collinear dipole-dipole and pole-dipole configurations over a dissipative layered subsurface, the percent frequency effects of electromagnetic coupling are seen to be as high as 60 percent for large $L^2(\sigma_1 f)$ values, where L is the length of the receiving dipole, σ_1 is the conductivity of the top layer of the half-space, and f is the higher frequency of excitation used. In both frequency and time-domain analyses, the distinctive effects of layering compared to that of a homogeneous half-space response are shown for different electrode configurations, layer geometry, and electrical parameters of the subsurface. The pole-dipole configuration of electrodes, in general,

exhibits higher coupling compared to the dipole-dipole configuration. In time-domain measurements, the late off-time transient decays reflect almost entirely the normal polarizability of the layered subsurface, in that the coupling responses are significant only during the early off-time of the transient.

The mutual impedance between grounded dipoles of arbitrary length is computed by extension of the complete solution of the boundary-value problem of a horizontal electric dipole situated over a multilayered half-space. A number of nomograms are presented for various layered structures to eliminate the electromagnetic coupling response in the induced-polarization measurements in order to obtain the true polarization effect of the subsurface.

INTRODUCTION

The mutual impedances of grounded wires are of prime importance in induced-polarization surveys used in mineral exploration. At low frequencies, the electromagnetic coupling and the normal polarization effect of the subsurface material have similar functional behavior with respect to the conductivity of the half-space, and their combined effect is recorded in an induced-polarization survey. To study the normal polarizability of a mineralized body in its true perspective, therefore, it is necessary to eliminate the effect of the electromagnetic coupling. In this paper, expressions for electromagnetic coupling have been developed, and computations are made for collinear arrays of transmitting and receiving dipoles of arbitrary length on the surface of a multilayered, conductive, and/or polarizable

half-space. Results are obtained in the frequency domain and in the time domain with any arbitrary pulse shape of the input current excitation.

Mutual impedances of wires of finite length on or above the surface of a uniform earth have been treated by Foster (1933) and for two-layer horizontal stratification by Riordan and Sunde (1933) and Hohmann (1970). The time-domain responses of various dipole sources over half-spaces have been considered by Bhattacharyya (1957, 1964) and Wait (1951, 1960). A review of the quantitative analysis of the transient electromagnetic exploration made in the USSR is presented by Vanyan (1967). In a recent paper, Millett (1967) published a table of electromagnetic coupling computed for a collinear dipole array on the surface of a homogeneous half-space. A quantitative interpretation scheme of transient electromag-

† Manuscript received by the Editor May 22, 1972; revised manuscript received September 8, 1972.

* University of California, Berkeley, California 94720.

© 1973 Society of Exploration Geophysicists. All rights reserved.

netic fields over a layered half-space has been developed by Morrison et al (1969). In many of these studies a number of approximations, including neglect of displacement currents in the ground, assumption of Laplace's equation for potentials in the air, etc., have been made. In layered models, and particularly in polarizable material, these conditions are not valid under certain circumstances.

To date, most of the time-domain coupling studies have been restricted to a uniform earth and a step-function excitation of the source. The availability of the fast Fourier transform algorithm of Cooley and Tukey (1965) has made it possible to consider any arbitrary shape of a repetitive pulse excitation in the present discussion.

Expressions for the mutual impedance for wires of finite length can be derived by integrating the electric field of horizontal electric dipoles situated over a uniform or layered half-space. At sufficiently low frequencies, the attenuation and phase difference along the transmitting and receiving wires may be neglected, and the electric field at a given point may be obtained by integration of the field intensities due to dipoles assumed to be located along the transmitting wire. The mutual impedance is obtained by integrating this field over the length of the receiving wire.

The solution of the boundary-value problem of a dipole source over a multilayered half-space has been obtained by developing an input admittance and input impedance concept in Hankel-transformed (cylindrical wavenumber λ) space. To achieve complete generality in the solution, all integrals in the expressions for the fields are defined without any assumption and are evaluated numerically. A brief outline of the development of the complete solution of the electromagnetic fields with a horizontal electric dipole situated on or above a stratified half-space is given below.

A source dipole moment density

$$M \left(M = \frac{-j\omega\mu_0 I ds}{4\pi k_0^2} \right)$$

directed along the x -axis is situated at a height d above a layered half-space as shown in Figure 1. Each of the laterally homogeneous layers is characterized by a conductivity σ_i , dielectric permittivity ϵ_i , and magnetic permeability μ_i . A time dependence of $e^{+j\omega t}$ for the source excitation is

assumed. An absence of symmetry of the source requires the boundary-value problem to be solved in terms of a Hertz potential $\bar{\pi}$ defined as

$$\bar{\pi} = \hat{e}_x \pi_x + \hat{e}_z \pi_z; \quad \pi_y = 0.$$

The electric and magnetic field vectors on or above the half-space can be obtained from the vector potential $\bar{\pi}$ as

$$\bar{E} = k_0^2 \bar{\pi} + \nabla(\nabla \cdot \bar{\pi}),$$

and

$$\bar{H} = (\sigma_0 + j\omega\epsilon_0)\nabla \times \bar{\pi}, \quad (1)$$

where $k_0^2 = \omega^2\mu_0\epsilon_0 - j\sigma_0\mu_0\omega$ is the propagation constant in the medium above the half-space.

The wave equation for the primary source potential $\bar{\pi}_p$ is given as

$$(\nabla^2 + k_0^2)\bar{\pi}_p = \bar{M}\delta(x)\delta(y)\delta(z-d), \quad (2)$$

with

$$r^2 = x^2 + y^2 + (z-d)^2 = \rho^2 + (z-d)^2.$$

A solution to the inhomogeneous Helmholtz equation (2) can be expressed in the Hankel-transformed space (λ -domain) by the Sommerfeld integral,

$$\begin{aligned} \pi_p &= M \frac{e^{-jk_0 r}}{r} \\ &= M \int_0^\infty \frac{\lambda}{\sqrt{\lambda^2 - k_0^2}} e^{-u_0|z-d|} J_0(\lambda\rho) d\lambda. \end{aligned} \quad (3)$$

The secondary vector potential $\bar{\pi}_s$, due to the presence of the half-space, satisfies, in the source-free region, the homogeneous wave equation

$$(\nabla^2 + k_i^2)\bar{\pi}_s = 0, \quad (4)$$

which has solutions of the form:

$$\begin{aligned} \pi_s &= A(\lambda) e^{\pm u_i z} \frac{J_n(\lambda\rho)}{Y_n(\lambda\rho)} \frac{\cos(n\phi)}{\sin(n\phi)}, \\ n &= 0, 1, 2, \dots \end{aligned} \quad (5)$$

where

$$u_i = \sqrt{\lambda^2 - k_i^2}.$$

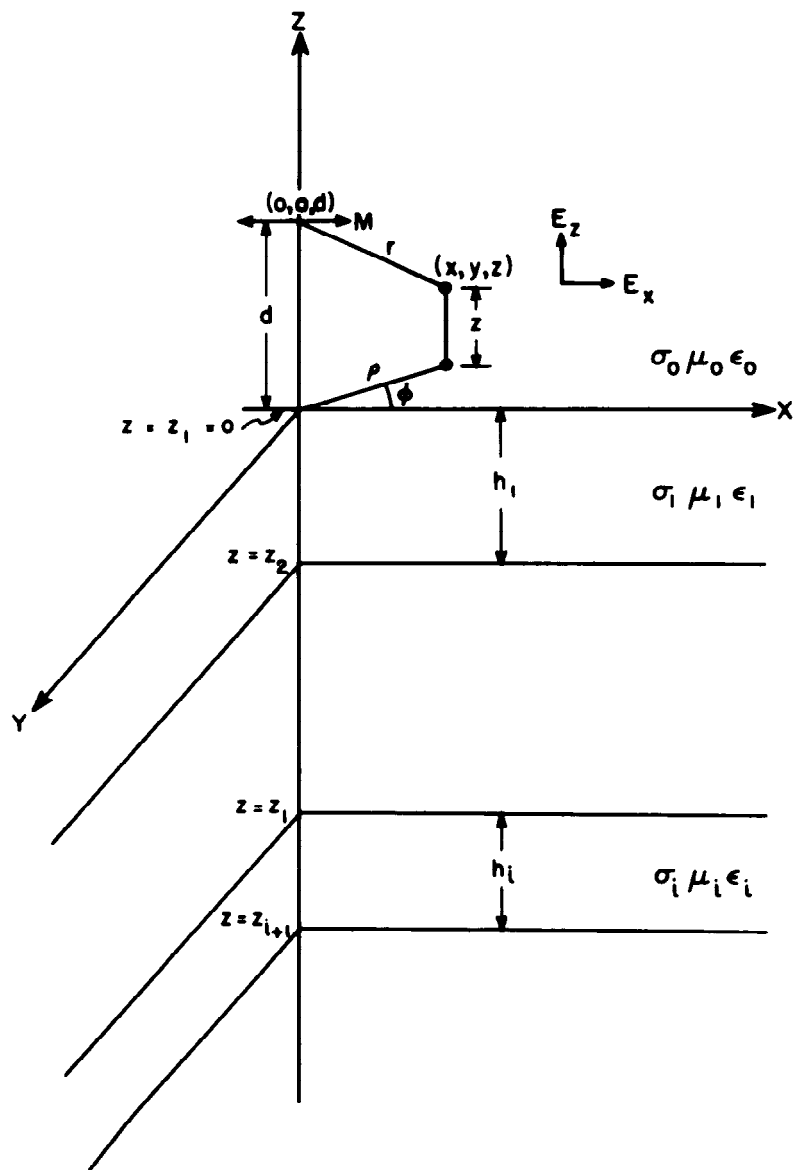


FIG. 1. Generalized orientation of a horizontal electric dipole above a multilayered earth.

To solve the potentials in the different regions of the multilayered half-space, boundary conditions, from the continuity of the normal and tangential E - and H -fields, have to be applied at each of the interfaces. Following this development, the potentials in the zone $d \geq z \geq 0$ above a generalized n -layered half-space can be written as (Dey and Ward, 1970; Dey et al, 1970)

$$\pi_z = M \int_0^\infty \left[\frac{\lambda}{u_0} e^{u_0(z-d)} + \frac{\lambda}{u_0} R_{TE}(\lambda) e^{-u_0(z+d)} \right] J_0(\lambda \rho) d\lambda, \quad (6)$$

and

$$\pi_z = M \frac{\partial}{\partial x} \int_0^\infty \left[\frac{R_{TE}(\lambda) + R_{TM}(\lambda)}{\lambda} \right] \cdot e^{u_0(z+d)} J_0(\lambda \rho) d\lambda, \quad (7)$$

where the reflection coefficient $R_{TM}(\lambda)$ for the transverse magnetic mode is given by Wait (1966) as

$$R_{TM}(\lambda) = \frac{I_0 - Z_1}{I_0 + Z_1},$$

in which

$$I_0 = \frac{u_0}{j\omega\epsilon_0},$$

and

$$Z_i = I_i \frac{Z_{i+1} + I_i \tanh(u_i h_i)}{I_i + Z_{i+1} \tanh(u_i h_i)} \quad \text{for } i = 1, 2, \dots, n-1$$

with

$$Z_n = I_n = \frac{u_n}{\sigma_n + j\omega\epsilon_n}.$$

Similarly, the reflection coefficient $R_{TE}(\lambda)$ for the transverse electric mode is given by Wait (1966) as

$$R_{TE}(\lambda) = \frac{N_0 - Y_1}{N_0 + Y_1},$$

in which

$$N_0 = \frac{u_0}{j\omega\mu_0},$$

and

$$Y_i = N_i \frac{Y_{i+1} + N_i \tanh(u_i h_i)}{N_i + Y_{i+1} \tanh(u_i h_i)} \quad \text{for } i = 1, 2, \dots, n-1,$$

with

$$Y_n = N_n = \frac{u_n}{j\omega\mu_n}.$$

Now, using equations (1), (6), and (7), the x -component of the electric field on the surface of the half-space (at $z=0$) can be obtained as

$$\begin{aligned} E_x &= k_0^2 \pi_x + \frac{\partial}{\partial x} \left(\frac{\partial \pi_x}{\partial x} + \frac{\partial \pi_z}{\partial z} \right) \Big|_{z=0} \\ &= M k_0^2 \int_0^\infty \left[\frac{\lambda}{u_0} + \frac{\lambda}{u_0} R_{TE}(\lambda) \right] J_0(\lambda \rho) d\lambda \\ &\quad + M \frac{\partial^2}{\partial x^2} \left[\int_0^\infty \left\{ \frac{\lambda}{u_0} + \frac{\lambda}{u_0} R_{TE}(\lambda) \right. \right. \\ &\quad \left. \left. - \frac{u_0}{\lambda} [R_{TE}(\lambda) + R_{TM}(\lambda)] \right\} J_0(\lambda \rho) d\lambda \right], \end{aligned} \quad (8)$$

which is expressed as

$$E_x = IdS \left[-P(\rho) + \frac{\partial^2 Q(\rho)}{\partial x^2} \right], \quad (9)$$

where

$$\begin{aligned} P(\rho) &= \frac{j\omega\mu_0}{4\pi} \\ &\quad \cdot \int_0^\infty \left[\frac{\lambda}{u_0} + \frac{\lambda}{u_0} R_{TE}(\lambda) \right] J_0(\lambda \rho) d\lambda, \end{aligned} \quad (10)$$

and

$$\begin{aligned} Q(\rho) &= \frac{-j\omega\mu_0}{4\pi k_0^2} \int_0^\infty \left[\frac{\lambda}{u_0} \{1 + R_{TE}(\lambda)\} \right. \\ &\quad \left. - \frac{u_0}{\lambda} \{R_{TE}(\lambda) + R_{TM}(\lambda)\} \right] J_0(\lambda \rho) d\lambda. \end{aligned} \quad (11)$$

For a homogeneous earth with a propagation constant k_1 of the lower half-space, these expressions can be reduced to the simpler forms given below.

$$P(\rho) = \frac{j\omega\mu_0}{4\pi} \int_0^\infty \frac{2\lambda}{(u_0 + u_1)} J_0(\lambda \rho) d\lambda, \quad (12)$$

and

$$\begin{aligned} Q(\rho) &= \frac{-j\omega\mu_0}{2\pi} \\ &\quad \cdot \int_0^\infty \frac{\lambda}{(k_1^2 u_0 + k_0^2 u_1)} J_0(\lambda \rho) d\lambda. \end{aligned} \quad (13)$$

At sufficiently low frequencies, if the application of the quasi-static approximation ($k_0 \rightarrow 0$; $u_0 \rightarrow \lambda$) is justified, the integrals $P(\rho)$ and $Q(\rho)$ can be evaluated analytically and are obtained as

$$P(\rho) = \frac{j\omega\mu_0}{4\pi} \int_0^\infty \frac{2\lambda}{(u_1 + \lambda)} J_0(\lambda\rho) d\lambda$$

$$= \frac{-j\omega\mu_0}{2\pi\rho} \left\{ \frac{1 - (1 + jk_1\rho)e^{-jk_1\rho}}{k_1^2\rho^2} \right\}, \quad (14)$$

and

$$Q(\rho) = \frac{-j\omega\mu_0}{2\pi} \int_0^\infty \frac{J_0(\lambda\rho)}{k_1^2} d\lambda = \frac{-j\omega\mu_0}{2\pi k_1^2\rho}. \quad (15)$$

The equation (14) is known as the Foster integral.

The mutual impedance between the collinear wire elements dS and ds lying in the plane $z=0$ is given (Sunde, 1967) as

$$dZ_{ss} = dSds \left[P(\rho) + \frac{\partial^2 Q(\rho)}{\partial S \partial s} \right]. \quad (16)$$

If the attenuation effect in the propagation along the transmitter and the receiver wires is

neglected, the mutual impedance of the transmitting wire S and the receiving wire s , expanding from A to B and a to b , respectively, as shown in Figure 2, is obtained by integrating the equation (16) as

$$Z_{ss} = \int_A^B \int_a^b \left[P(\rho) + \frac{\partial^2 Q(\rho)}{\partial S \partial s} \right] dS ds, \quad (17)$$

and the voltage observed at the receiving dipole is

$$V(\omega) = I(\omega) \cdot Z_{ss}(\omega). \quad (18)$$

The integrations involving the function $Q(\rho)$ can be evaluated by inserting the four limits that are the distances between the wire terminals, since each of the indicated integrations has a corresponding differentiation. Then, Z_{ss} can be written as

$$Z_{ss} = Q(Aa) - Q(Ab) + Q(Bb) - Q(Ba) + I_{ss}, \quad (19)$$

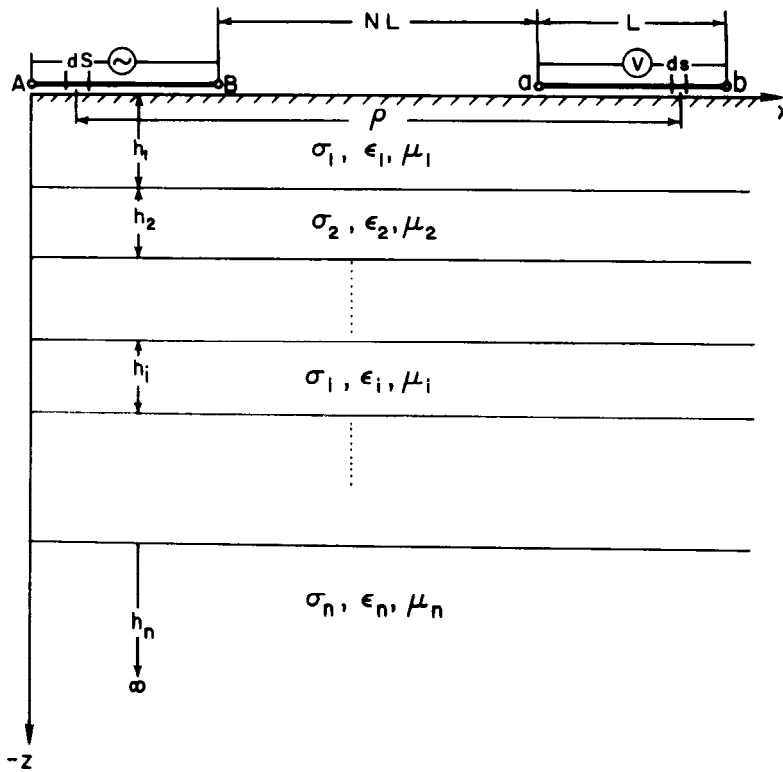


FIG. 2. The transmitter and the receiver dipole setup above a layered earth.

where

$$L_{Ss} = \int_A^B \int_a^b P(\rho) dS ds.$$

The functions $Q(\rho)$ and $P(\rho)$ are generally complex valued and in the limit $\rho \rightarrow \infty$, $Q(\rho) \rightarrow 0$, and $P(\rho) \rightarrow 0$. A detailed treatment of their behavior with various relative orientations of the wires is given by Sunde (1967).

At zero frequency, the function L_{Ss} vanishes, and the direct current mutual resistance Z_{Ss}^{dc} is given by

$$Z_{Ss}^{\text{dc}} = Q^{\text{dc}}(Aa) - Q^{\text{dc}}(Ab) + Q^{\text{dc}}(Bb) - Q^{\text{dc}}(Ba), \quad (20)$$

where the function $Q^{\text{dc}}(\rho)$ for an n -layered half-space is defined by Sunde (1967) as

$$Q^{\text{dc}}(\rho) = \frac{1}{2\pi\sigma_1} \int_0^\infty K_{1,2,\dots,n}(\lambda) J_0(\lambda\rho) d\lambda, \quad (21)$$

in which

$$\begin{aligned} K_{1,2,\dots,n}(\lambda) &= \frac{1 - \psi_{1,2,\dots,n} e^{-2\lambda d_1}}{1 + \psi_{1,2,\dots,n} e^{-2\lambda d_1}}; \\ \psi_{1,2,\dots,n} &= \frac{\left(\frac{1}{\sigma_1}\right) - \left(\frac{1}{\sigma_2}\right) K_{1,2,3,\dots,n}}{\left(\frac{1}{\sigma_1}\right) + \left(\frac{1}{\sigma_2}\right) K_{1,2,3,\dots,n}}; \\ K_{(m-1),m,\dots,n} &= \frac{1 - \psi_{(m-1),m,\dots,n} e^{-2\lambda d_{m-1}}}{1 + \psi_{(m-1),m,\dots,n} e^{-2\lambda d_{m-1}}}; \\ \psi_{(m-1),m,\dots,n} &= \frac{\left(\frac{1}{\sigma_{m-1}}\right) - \left(\frac{1}{\sigma_m}\right) K_{m,(m+1),\dots,n}}{\left(\frac{1}{\sigma_{m-1}}\right) + \left(\frac{1}{\sigma_m}\right) K_{m,(m+1),\dots,n}}; \\ &\vdots \\ K_{(n-1),n} &= \frac{1 - \psi_{(n-1),n} e^{-2\lambda d_{n-1}}}{1 + \psi_{(n-1),n} e^{-2\lambda d_{n-1}}}; \end{aligned}$$

and

$$\psi_{(n-1),n} = \frac{\left(\frac{1}{\sigma_{n-1}}\right) - \left(\frac{1}{\sigma_n}\right)}{\left(\frac{1}{\sigma_{n-1}}\right) + \left(\frac{1}{\sigma_n}\right)}.$$

Following the representation of the induced-polarization survey in the *frequency domain*, the percent frequency effect (PFE) of the mutual electromagnetic coupling is then defined as

$$\text{PFE} = \left[1 - \left\{ \frac{|Z_{Ss}|}{Z_{Ss}^{\text{dc}}} \right\} \right] 100 \text{ percent.} \quad (22)$$

The theoretical development given above for a harmonic excitation of the source can be used to obtain the time-domain mutual coupling response. The discrete Fourier spectrum or Fourier series expansion of the periodic input pulse is used for the purpose. For each harmonic in the Fourier series expansion of the pulse ω_j ($j=0, 1, 2, \dots, N$),

the transfer function $Z_{ss}(\omega_j)$ is multiplied by the corresponding complex amplitude $I(\omega_j)$ of the current pulse, and the resulting voltage in time is obtained by the summation of this product over all harmonics. In the present study, the Fourier amplitudes of the arbitrary input pulse are obtained by using the fast Fourier transform (FFT) algorithm. Mutual impedances for the wires over the layered half-space are then obtained at each of the harmonics and the product $V(\omega_j) = I(\omega_j) \cdot Z_{ss}(\omega_j)$ is inverse-transformed, using the FFT to obtain the time function.

A number of input-current excitation pulse shapes used in this study are shown in Figure 3. The maximum current in each of the pulses is assumed to be 1 amp.

NUMERICAL METHODS USED IN THE COMPUTATIONS

The integral functions $Q(\rho)$ and $P(\rho)$ used to define the mutual impedance are, in general, quite complex, and no analytical solutions to these integrals valid for the entire range of integration have been presented so far. For a homogeneous half-space and at very low frequencies, analytic solutions exist, and these are indicated in equations (14) and (15). To compute the response over

any layered model, therefore, numerical techniques have to be used to yield a high degree of accuracy.

In the equations (10) and (11), the kernels of the integrals are modulated by a Bessel function of the zeroeth order. A scheme devised to solve these integrals has been to approximate the integrand in each half-cycle of the Bessel function by a 15th-order or a 31st-order polynomial by using the method of 8-point or 16-point Gaussian quadrature, respectively. Thus, a series of decreasing values of alternating signs of integrals is obtained. This series is usually of 20 to 40 terms and a modified Euler transformation is applied to the series for improved convergence until an accuracy of 0.01 percent is achieved. For very low values of λ in the first few half-cycles of the integrand, at times even the 16-point Gaussian quadrature does not yield the accuracy desired, and the integration is performed by the trapezoidal rule together with Romberg's extrapolation method using up to 2^{10} sample points. The sum of the series yields an approximation to the integral with a high degree of accuracy (usually 0.01 percent).

The function L_{ss} in equation (19) involves a double integration over $P(\rho)$. This is effected by

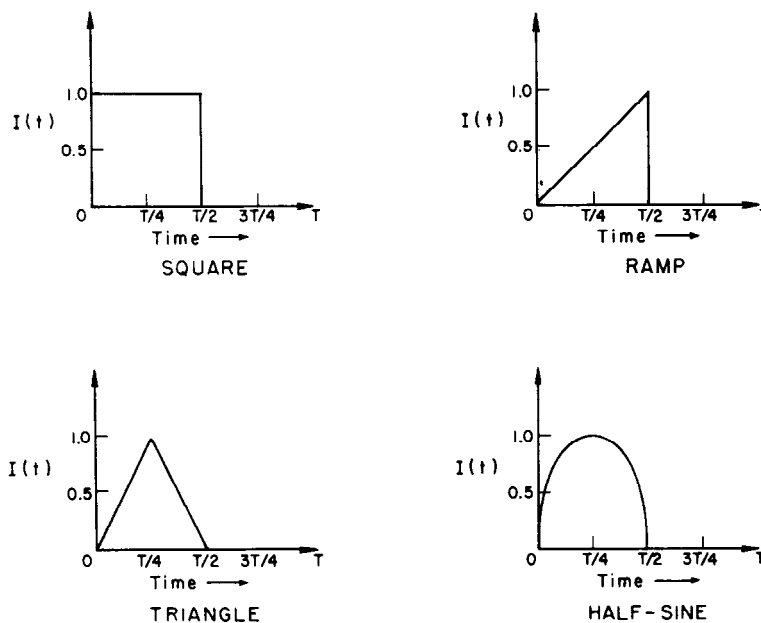


FIG. 3. Input-current excitation pulse shapes.

using a double-summation series approximation with variable indices of summation, or by using the method of Simpson's 3-point rule. For the low frequencies of interest in this study, sufficient accuracy is attained by using the Simpson's rule.

The spectrum of an arbitrary square-wave pulse shape is in general not band-limited, and the convergence of the Fourier series with the harmonics is rather slow. As a result, some truncation effects are observed when the time responses of the product of FFT of the input current pulse and the mutual impedance at the corresponding frequency, is inverse transformed. Since the pulse spectrum is, in general, not band-limited, the FFT is not asymptotic to the analytic Fourier transform of the pulse, irrespective of how small a sampling interval is used. Also, since the mutual impedance at high frequency does not actually become zero, the corresponding voltage function is sharply truncated. The truncation together with the inadequacy in sampling may yield a high-frequency Nyquist ripple on the time-domain response. This situation can sometimes be improved upon by using a Hanning smoothing function on the FFT of the input pulse, thus, forcing it to be band-limited. An additional noise is introduced in the time-domain response for high resistivities of the half-space and long off-times, when the signal drops off sharply, and a random pattern in the data may result from the predominance of computer round-off noise over the signal.

In all computations involving the homogeneous half-spaces in the time domain, the FFT algorithm was used with 2^{10} sample points for the total (on+off) time of the pulse. For layered models this number has been reduced in the light of the economics of the computation.

RESULTS

The frequency and time responses for a number of representative models have been computed. Two arrangements of the collinear transmitting and receiving dipoles are studied—one with equal length for each dipole, designated as the dipole-dipole configuration and the other with a transmitting dipole 50 times the length of the receiving dipole, designated as the pole-dipole configuration. Various parameters of the model, e.g., conductivities, thickness, and number of layers, have been varied to illustrate the general characteristics of the electromagnetic coupling over a uniform

or a multilayered half-space. In all of the following results, the magnetic permeability and the dielectric permittivity of the subsurface strata are assumed to be identical to those of the free-space.

Frequency-domain analysis

Homogeneous half-space response.—For very low frequencies ($f \leq 5$ Hz) used in standard induced-polarization surveys, the electromagnetic coupling response of the layered subsurface is found to be invariant with respect to the parameter $L^2(\sigma_1 f)$; L is the length of the receiving dipole; σ_1 , the conductivity of the top layer; and f the high frequency used in the survey. Thus, for the frequency-domain induced-polarization survey, the electromagnetic coupling can be obtained for any combination of L , σ_1 , and f using the computed templates described in the following discussion. A range of $10 \leq L^2(\sigma_1 f) \leq 10^5$ would, in general, include most induced-polarization surveys conducted over a host of geologic situations and a wide range of conductivities encountered in practical exploration.

The amplitude of the mutual impedance between the transmitting and the receiving dipoles in a dipole-dipole configuration located on the surface of a homogeneous earth of conductivity is illustrated in Figure 4. The amplitude of the mutual impedance is normalized by $Z_0^{dc} = 1/(2\pi\sigma L)$. Various dipole separations of $N = 1, 2, 3, 4, 5$ over a range of $10 \leq L^2(\sigma f) \leq 10^6$ have been considered. In the lower range of $L^2(\sigma f)$, the mutual impedance has the effect of lowering the apparent resistivity and is similar to the normal polarization effect expected of a mineralized inhomogeneity. However, for higher values of $L^2(\sigma f)$, this trend decreases as $|Z_{ss}/Z_0^{dc}|$ increases. In some layered models, $|Z_{ss}/Z_0^{dc}|$ for $L^2(\sigma f) > 10^5$ asymptotes to a value that is higher than the dc asymptote observed for low values of $L^2(\sigma f)$, thereby giving rise to negative PFE effects.

The phase of the mutual impedance between the transmitting and the receiving dipoles in a dipole-dipole configuration situated on the surface of a homogeneous earth is illustrated in Figure 5. For low values of $L^2(\sigma f)$, the phase of (Z_{ss}/Z_0^{dc}) remains essentially the same as at dc. For $L^2(\sigma f) > 10^3$, the phase deviation increases, the increase being greater for larger dipole separations. The phase anomalies are at their largest in the range

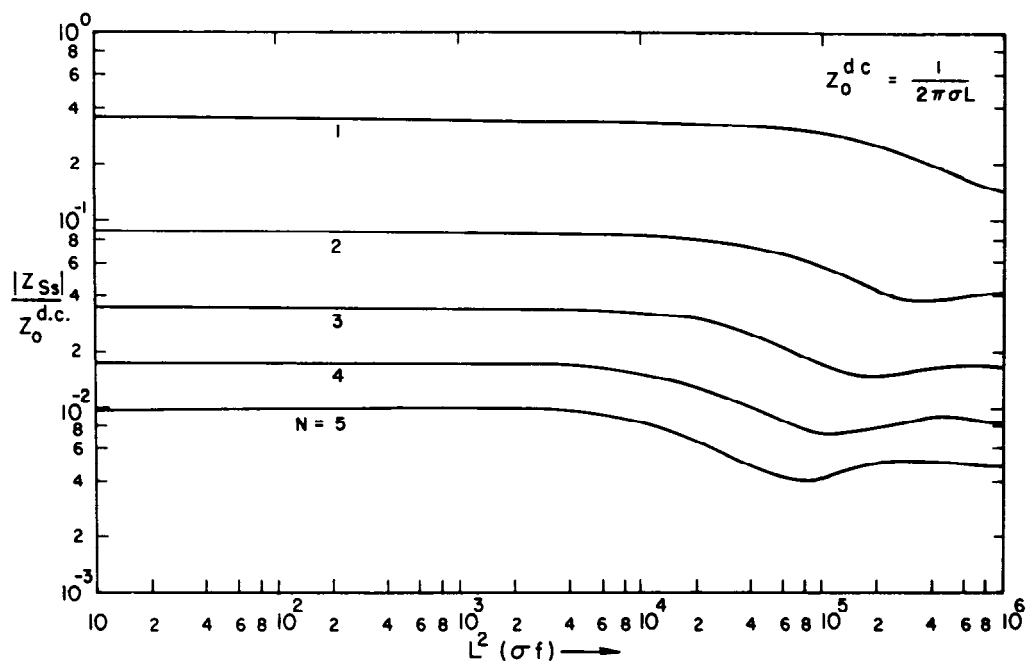


FIG. 4. Amplitude of normalized mutual impedance for a dipole-dipole configuration over a homogeneous earth.

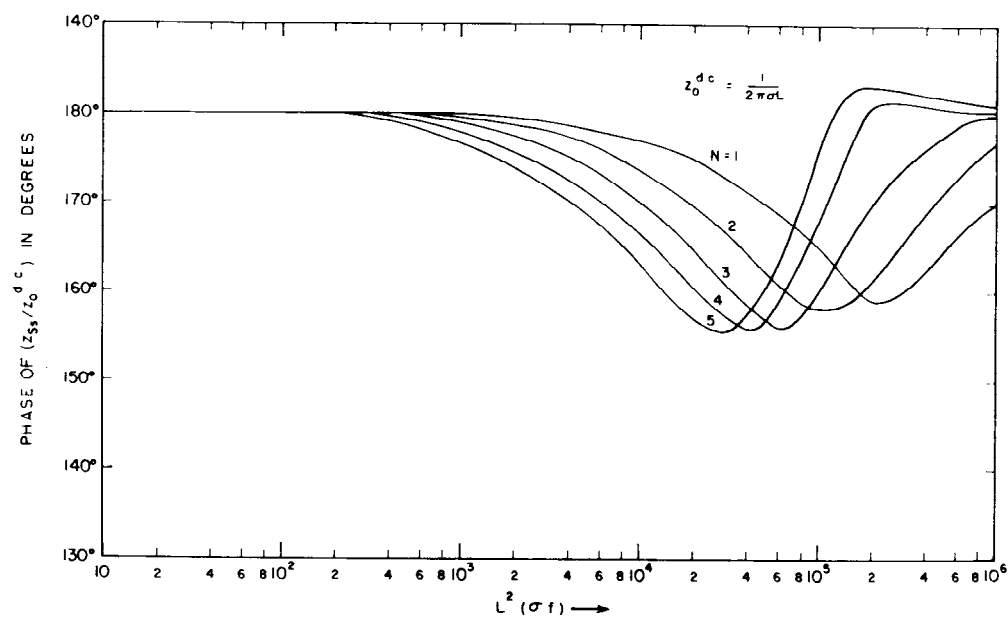


FIG. 5. Phase of normalized mutual impedance for a dipole-dipole configuration over a homogeneous earth.

$10^4 \leq L^2(\sigma f) \leq 10^5$ and decrease as $L^2(\sigma f)$ is increased. The phase response of the mutual impedance indicates the possibility of coherent detection of PFE due to electromagnetic coupling. However, for most practical ranges of $L^2(\sigma f)$ currently used in induced-polarization surveys, this phase-shift due to coupling is not significantly diagnostic, and in all of the following analyses the PFE is defined in terms of the amplitude of (Z_{ss}/Z_0^{dc}) .

Figures 6 and 7 illustrate the percent frequency effect (PFE) of mutual coupling over homogeneous half-spaces of various conductivity and dipole lengths in the range $10^2 \leq L^2(\sigma f) \leq 10^5$ using the dipole-dipole and the pole-dipole configurations, respectively. For low $L^2(\sigma f)$ values, there is an almost linear increase in coupling for both dipole-dipole and pole-dipole configurations. For high values of $L^2(\sigma f)$, however, this function becomes nonlinear, as a saturation effect is achieved for each of the dipole separations considered. This is explained by a deviation in the

mutual impedance functional response with frequency from the normal polarization effect, in that it increases following the monotonous decrease at lower frequencies. For the same value of $L^2(\sigma f)$, the PFE due to coupling is greater with larger dipole separations. For the range $L^2(\sigma f) < 10^4$, the coupling effect is significantly higher for the pole-dipole configuration, and the saturation effect for each dipole separation is apparently reached for a lower value of $L^2(\sigma f)$ for the pole-dipole than the dipole-dipole configuration.

Layered half-space responses.—A number of standard templates computed to evaluate the electromagnetic coupling effect over a two-layered earth with a top-layer thickness of $h_1/L = 0.25$ and conductivity contrasts $K = \sigma_2/\sigma_1 = 0.10$ and 10.0 are illustrated in Figures 8 through 11. Both dipole-dipole and pole-dipole configurations have been studied. In the range $10^2 \leq L^2(\sigma f) \leq 10^5$, for the two-layered models with a conductive overburden underlain by a resistive half-space

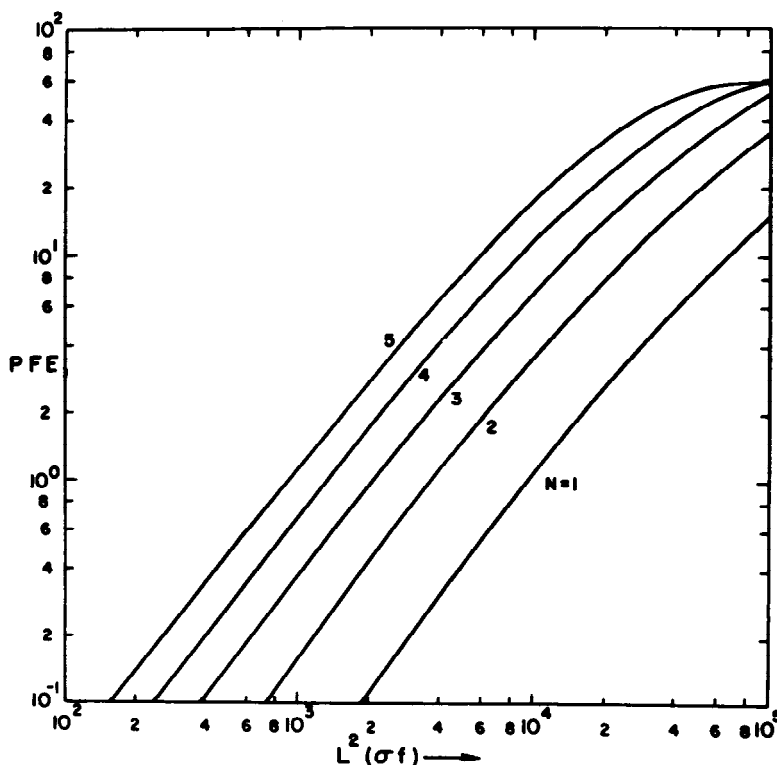


FIG. 6. Percent frequency effect for a dipole-dipole configuration over a homogeneous earth.

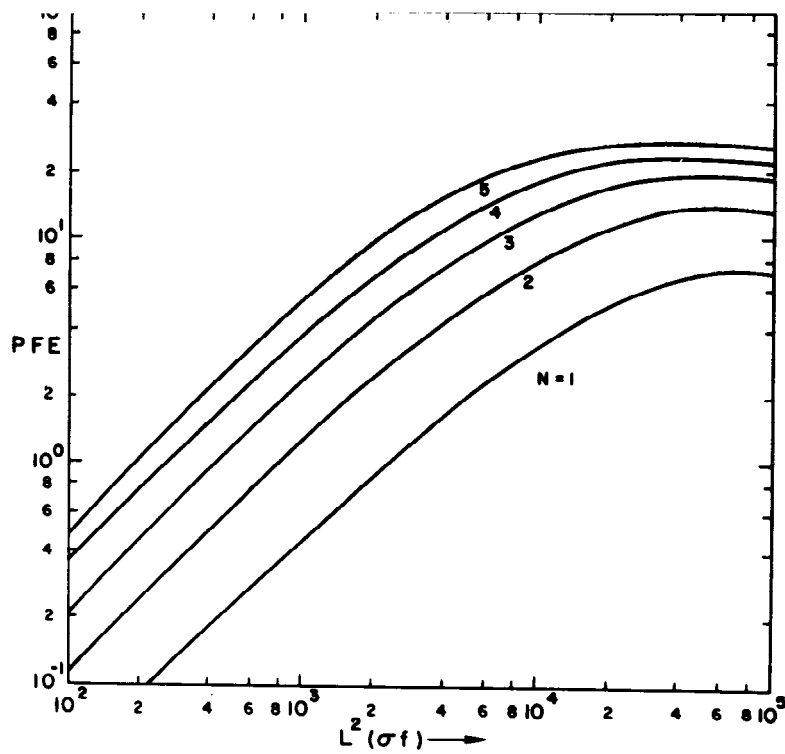


FIG. 7. Percent frequency effect for a pole-dipole configuration over a homogeneous earth.

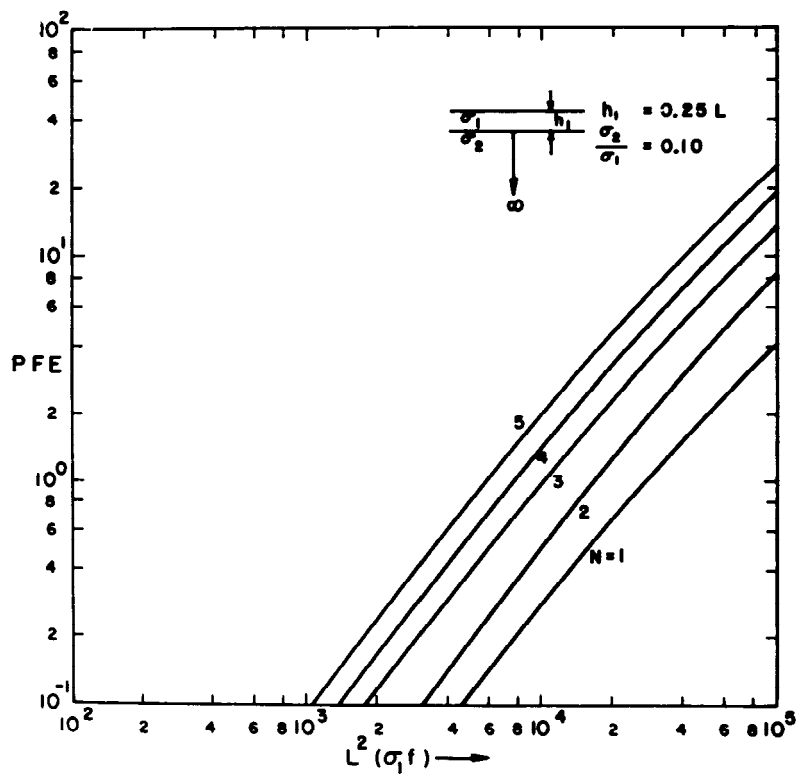


FIG. 8. Percent frequency effect for a dipole-dipole configuration over a two-layered earth model.

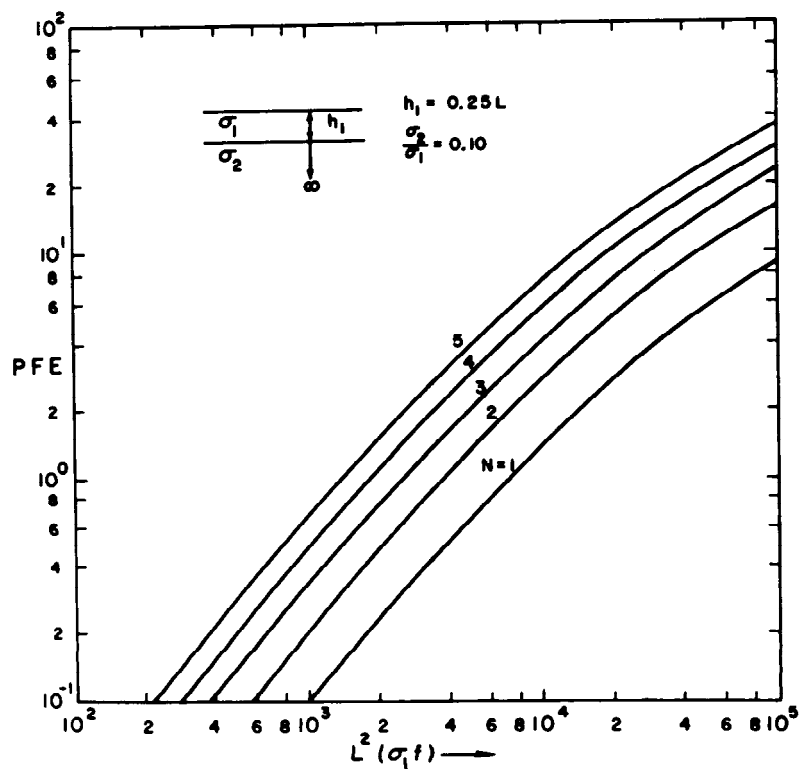


FIG. 9. Percent frequency effect for a pole-dipole configuration over a two-layered earth model.

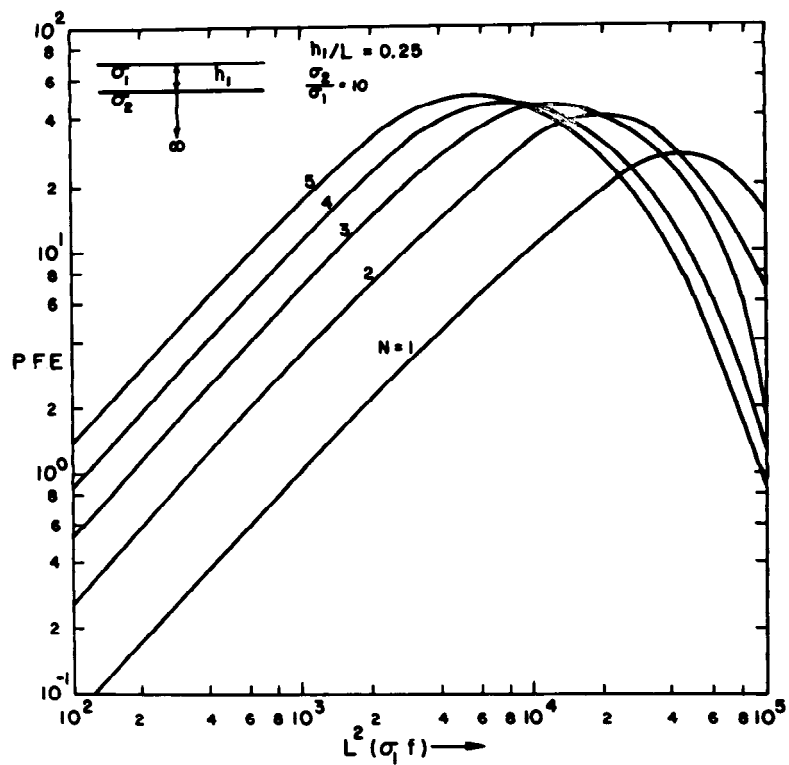


FIG. 10. Percent frequency effect for a dipole-dipole configuration over a two-layered earth model.

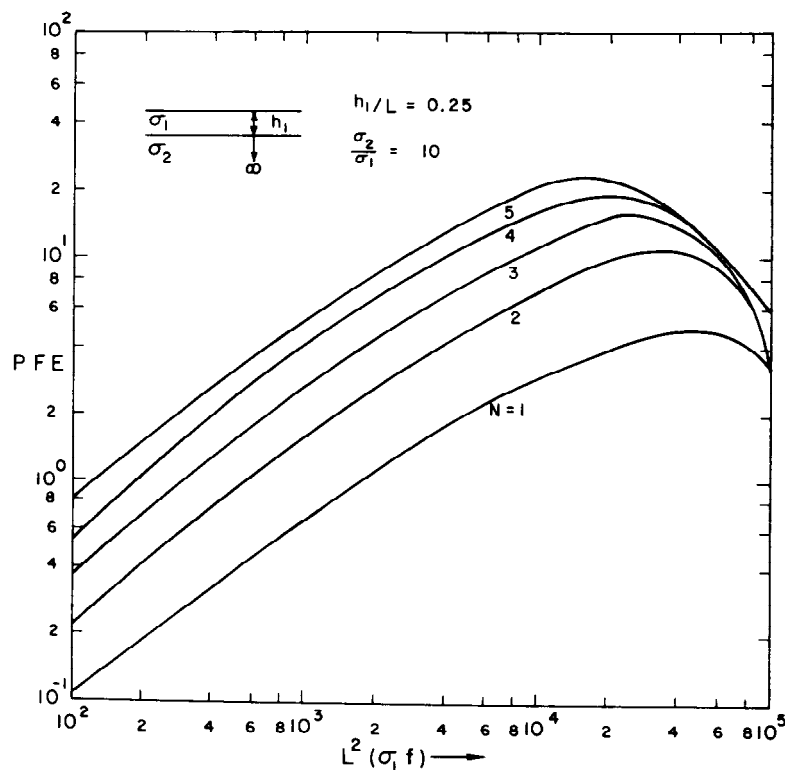


FIG. 11. Percent frequency effect for a pole-dipole configuration over a two-layered earth model.

($K=0.10$), the PFE due to coupling are substantially higher for the pole-dipole configurations for each dipole separation considered. In addition, these layered responses are generally lower than those obtained for a homogeneous earth with the top-layer conductivity for both configurations. For the layered case with $K=10.0$, when a resistive layer overlies a more conductive half-space, the coupling responses are higher than those of the homogeneous half-space with top-layer conductivity for $L^2(\sigma_1 f) < 10^4$ for both configurations. In addition, while the PFE due to coupling is higher for the pole-dipole configuration for lower values of $L^2(\sigma_1 f)$, for $L^2(\sigma_1 f) > 2 \times 10^3$, the reverse effect is observed. For $L^2(\sigma_1 f) > 5 \times 10^3$, the coupling effect is sharply reduced for both configurations considered since the $|Z_{ss}/Z_0^{\text{dc}}|$ values tend to saturate to the high-frequency asymptote which approaches or exceeds the dc asymptotes of $|Z_{ss}/Z_0^{\text{dc}}|$ for higher $L^2(\sigma_1 f)$ values.

The electromagnetic coupling responses with a dipole-dipole configuration over a three-layered earth with $\sigma_1:\sigma_2:\sigma_3=10:1:5$ and $h_1/L:h_2/L:h_3/L$

$=0.10:0.10:\infty$, for different dipole separations are shown in Figure 12. It is to be observed that for low values of $L^2(\sigma_1 f)$, the increasing trends of the PFE for the homogeneous half-space and the layered models are very similar, and an equivalent apparent resistivity of the half-space may be determined by shifting the response curves along the $L^2(\sigma_1 f)$ axis and matching with the homogeneous responses.

Effect of varying conductivity contrasts.—Figures 13 and 14 illustrate the effect of varying the ratio of σ_2/σ_1 on the electromagnetic coupling for the dipole-dipole and the pole-dipole configurations, respectively. The top layer thickness of a two-layer model is held constant at $h_1/L=0.10$, and the results corresponding to a dipole separation of $N=4$ for various σ_2/σ_1 values are illustrated. A relative comparison with the homogeneous half-space response indicates that the layered response is generally lower than the uniform earth for $K<1$ and higher for $K>1$ for both dipole configurations. In addition, for the range of $L^2(\sigma_1 f)$

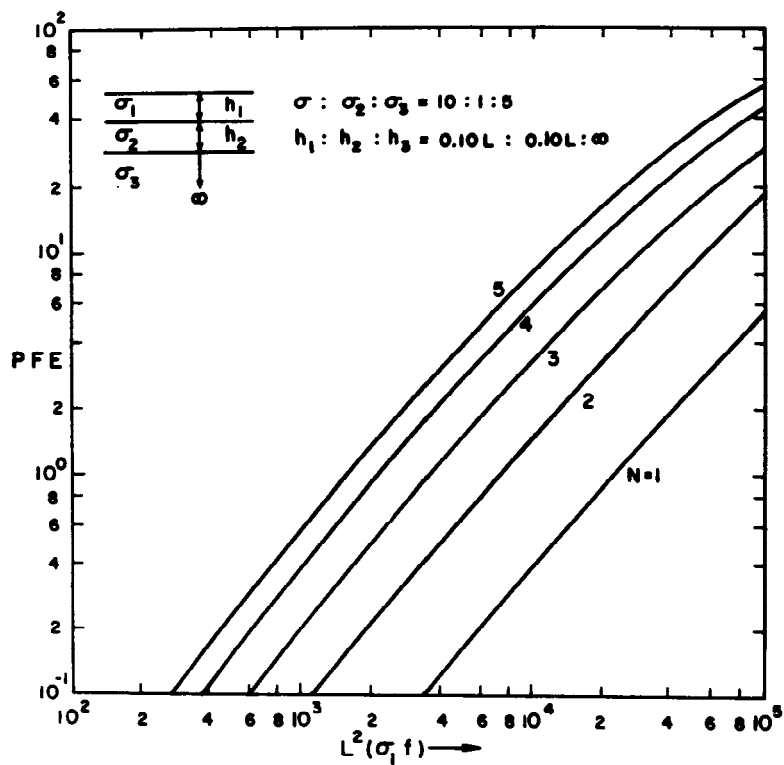


FIG. 12. Percent frequency effect for a dipole-dipole configuration over a three-layered earth model.

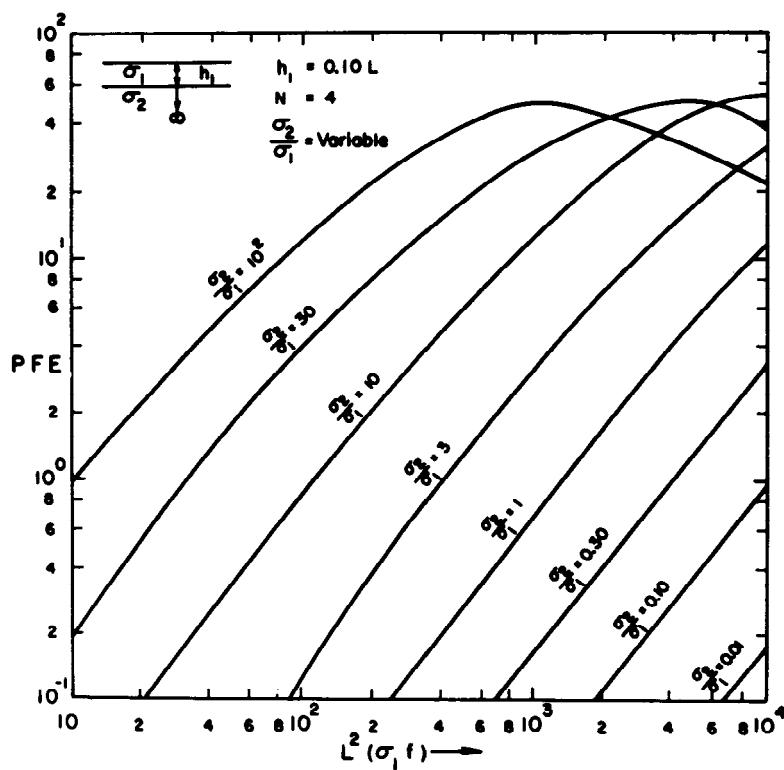


FIG. 13. Percent frequency effect for a dipole-dipole configuration over two-layered earth models of varying conductivity contrasts.

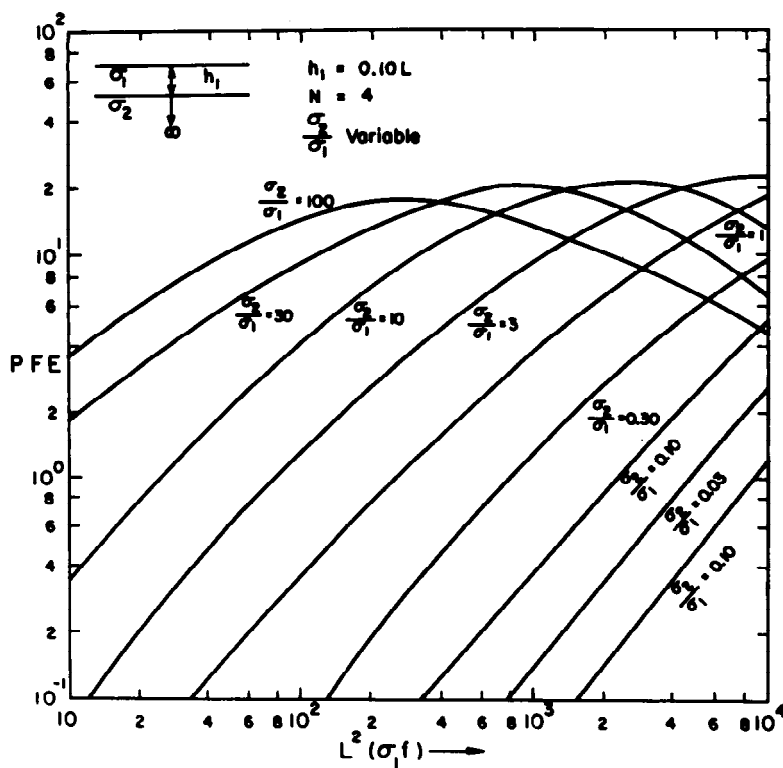


FIG. 14. Percent frequency effect for a pole-dipole configuration over two-layered earth models of varying conductivity contrasts.

considered, the pole-dipole configuration's coupling effect is consistently higher than the dipole-dipole configuration for $K < 1$, while for models with $K > 1$, this is true only for the lower range of $L^2(\sigma_1 f)$. For high values of $L^2(\sigma_1 f)$ (with $K > 1$) the fall-off in the coupling effect is sharper for the pole-dipole configuration. Substantial effects of layering can be seen even for values of K as small as 3.0 or 0.30, and no saturation effects are evident for $K = 100$ or 0.01.

Effect of varying layer thickness.—The coupling responses over a two-layered earth model with $\sigma_2/\sigma_1 = 0.10$ and 10.0 for the dipole-dipole configuration are illustrated in Figures 15 and 16 for different thicknesses of the top layer. The results shown correspond to a dipole separation $N = 4$. For the layered model with $\sigma_2/\sigma_1 = 0.10$, a gradual transition of the layered response to those of the homogeneous half-space cases are observed as h_1/L is varied. The effect of increasing h_1/L is that of increasing the coupling PFE for the range

of $L^2(\sigma_1 f)$ considered. For the two-layered model with a more conductive second layer ($\sigma_2/\sigma_1 = 10.0$), however, the effect observed is predominantly due to the second layer until the top layer attains a thickness of $h_1/L = 1.00$ when its effects become apparent. For greater top-layer thickness, the response asymptotes to that of the homogeneous earth with the conductivity of the top layer.

Time-domain analysis

The time-domain electromagnetic coupling effect has been studied by computing the voltage recorded at the receiving dipole during the on- and off-time of the current pulse applied to the transmitting dipole. A ratio of the transient (off-time) response to the steady-state on-time response is indicative of the coupling effect of the underlying half-space. In most of the following discussion, unless otherwise specified, a periodic square-wave shaped input-current excitation with 2 sec each of on- and off-time is assumed. The receiving dipole length has been maintained at

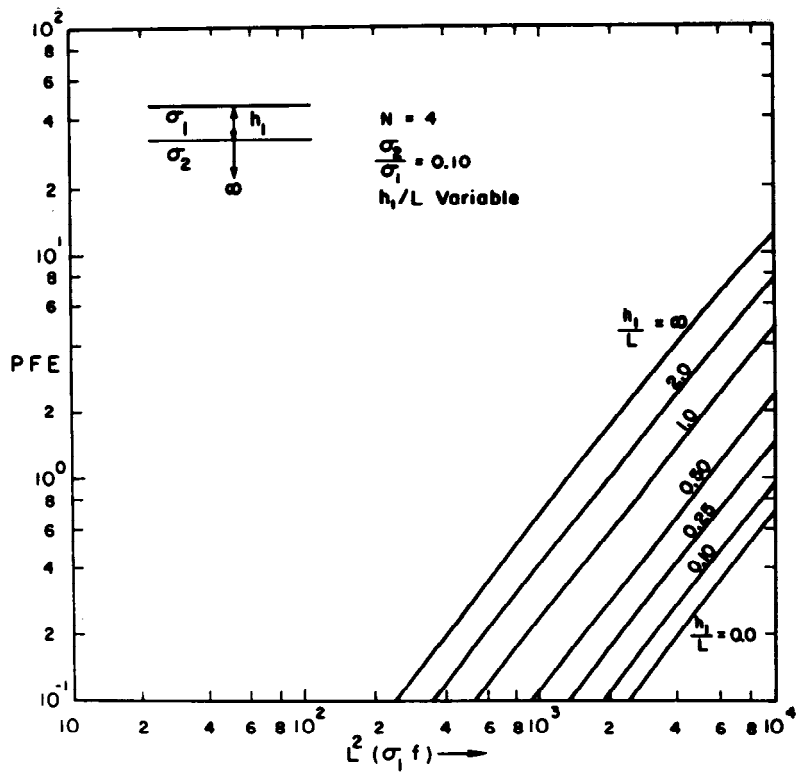


FIG. 15. Percent frequency effect for a dipole-dipole configuration over two-layered earth models of varying top-layer thicknesses.

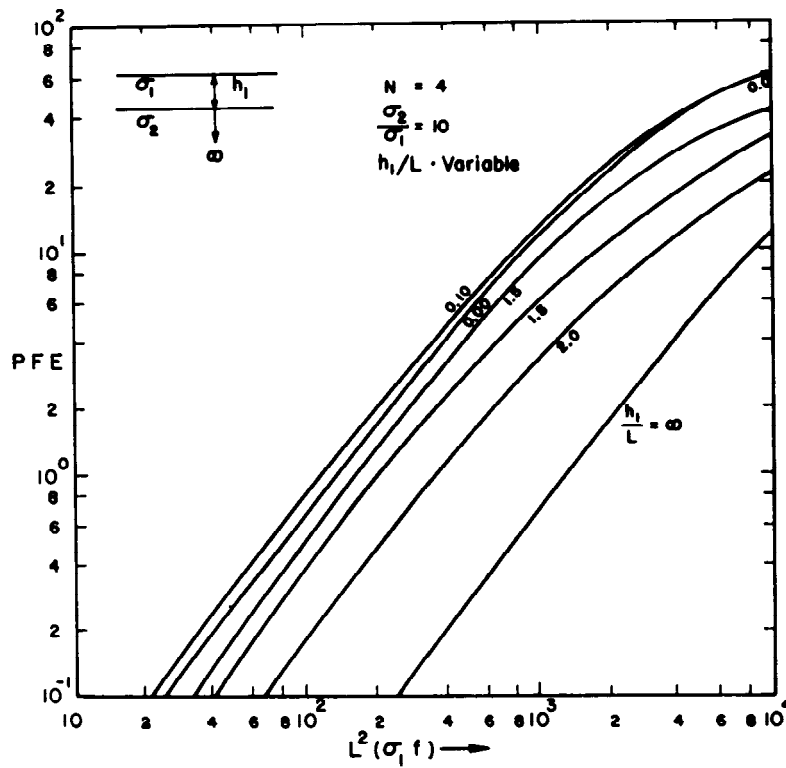


FIG. 16. Percent frequency effect for a dipole-dipole configuration over two-layered earth models of varying top-layer thicknesses.

400 m. In the latter segment of the following analysis the effects of varying the input-current pulse shape, the lengths of the receiving dipole, and the total time of the input pulse are also studied.

For all computations pertaining to a homogeneous earth model the 2^{10} sample points have been used for the total (on + off) time of the input current pulse. In the analyses of the layered earth models, however, 2^7 or 2^8 sample points are found to be sufficient to determine a smooth, repeatable transient decay.

Homogeneous half-space response.—The relative decays of the transient responses for different dipole separations ($N=1, 2, 3, 4, 5$) over a uniform earth of resistivity 100 ohm-m, for the dipole-dipole and the pole-dipole configuration are illustrated in Figures 17 and 18, respectively. As would be normally expected, the coupling responses are higher for longer wires used at larger dipole separations. For longer off-times, the trend of the decay of the transient, for both the dipole-dipole and the pole-dipole configurations are almost identical for the different dipole separations.

This, however, is anticipated since the low-frequency components predominate at long off-times, and an almost identical trend in the coupling PFE function is observed at low frequencies (refer to Figures 6 and 7) over a homogeneous earth. For short off-times, however, the decay rates are markedly different for different N values being progressively sharper for lower dipole separations. A comparison between Figures 17 and 18 at long off-times indicates a relative decay voltage almost ten times higher for the pole-dipole than the dipole-dipole configuration. This too is explained in the light of relatively higher mutual impedance of the pole-dipole configurations observed in the frequency domain over most of the frequency range of interest.

Effect of varying the resistivity of the homogeneous earth.—The transient decay patterns as observed for a dipole separation $N=2$ and various resistivities of the uniform half-space, for the dipole-dipole and the pole-dipole configurations, are shown in Figures 19 and 20, respectively. As is observed from the low mutual impedances $|Z_{ss}/Z_0^{dc}|$ for higher resistivities of the half-space

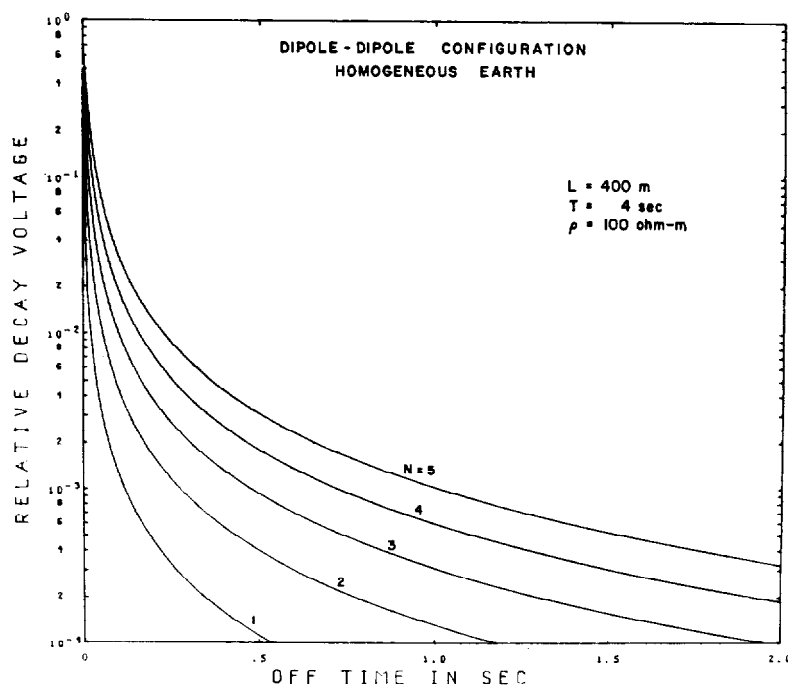


FIG. 17. Time-domain coupling response for a dipole-dipole configuration over a homogeneous earth.

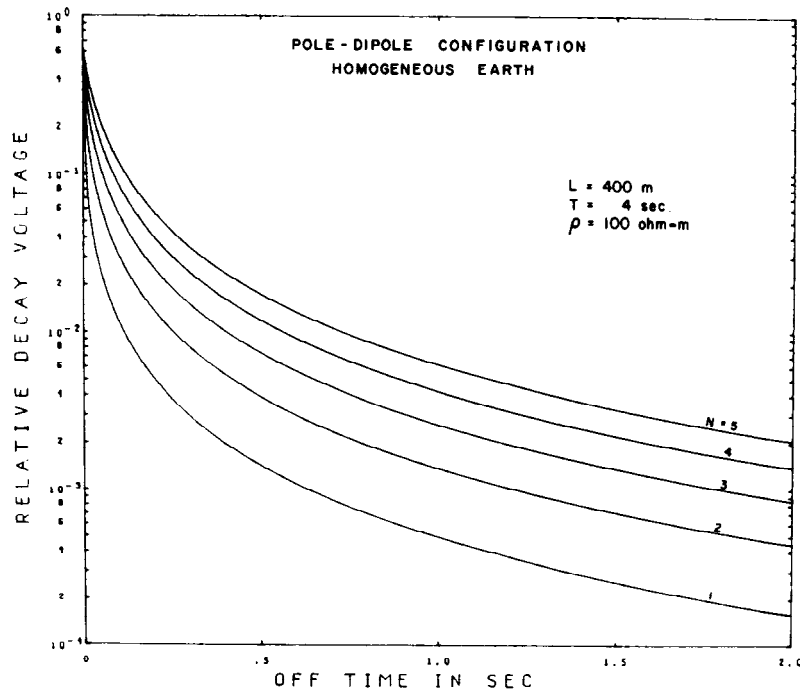


FIG. 18. Time-domain coupling response for a pole-dipole configuration over a homogeneous earth.

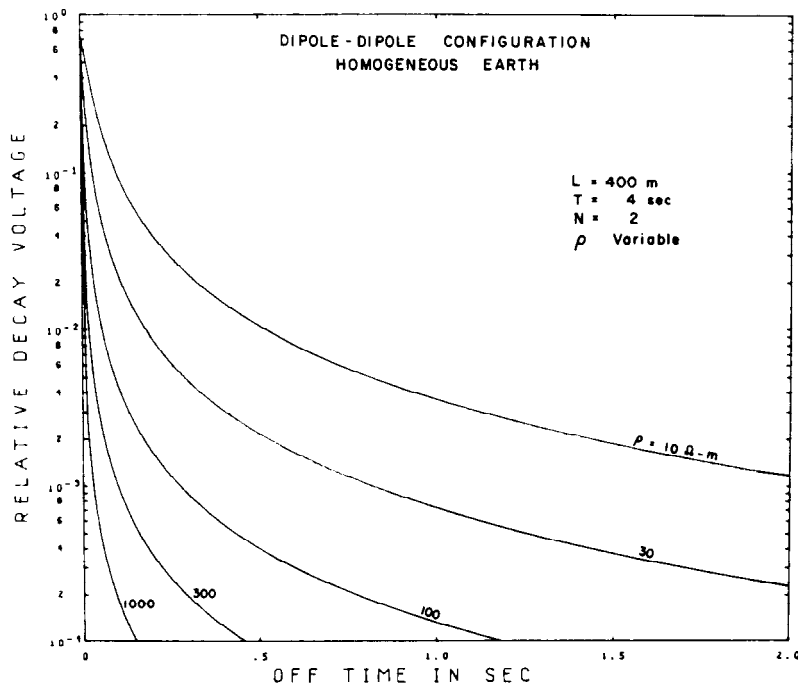


FIG. 19. Time-domain coupling response for a dipole-dipole configuration over homogeneous earth models of varying resistivity.

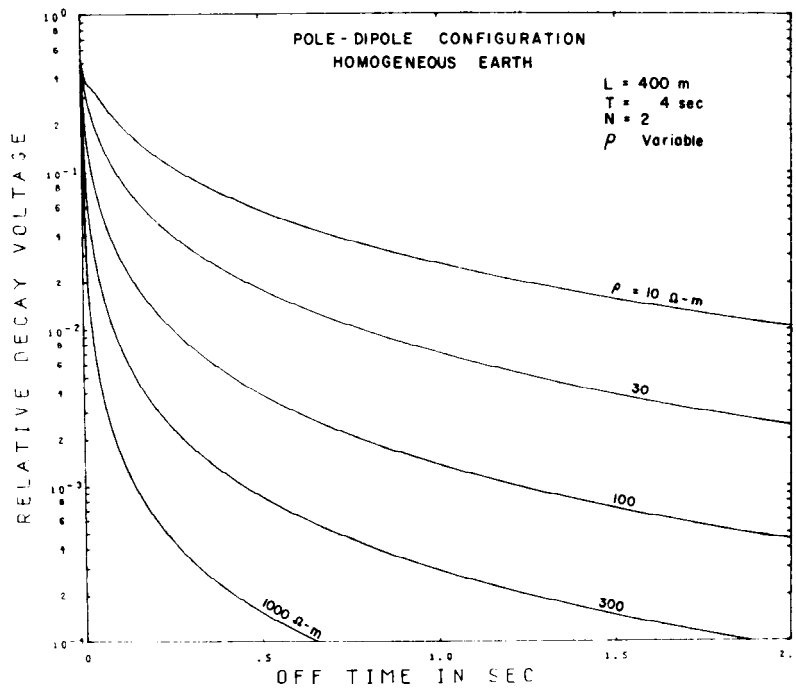


Fig. 20. Time-domain coupling response for a pole-dipole configuration over homogeneous earth models of varying resistivity.

in the frequency domain, the relative transient voltages decrease as the half-space resistivity is increased. The relative sharpness of the decay involving the short off-times ($T_{off} < 1.0$ sec) also increases with increase in the resistivity for both configurations. The decay rate for different dipole separations is faster for the dipole-dipole compared to the pole-dipole configuration.

Effect of varying the dipole length.—Figure 21 illustrates the relative transient decay voltages for a dipole separation $N=3$ over a homogeneous earth of resistivity 100 ohm-m for various lengths of the receiving dipole. The electrode configuration employed is that of the dipole-dipole. The increase in the coupling effect is significant as the dipole length is increased from 100 m to 1000 m. While the coupling effect for $T_{off} > 1.0$ is insignificant for $L < 200$ m, the relative decay voltage remains at a rather large value for longer dipoles. The selection of a proper value of L is of prime significance in an induced-polarization survey, in that the larger the L , the greater the depth of exploration. However, Figure 21 indicates that

for a normally resistive ground ($\rho=100$ ohm-m), the coupling response with large L at long off-times may overshadow the normal polarization decay of a mineralized inhomogeneity.

Layered half-space responses.—The relative transient decay voltages for different dipole separations ($N=1, 2, 3, 4, 5$) over a two-layered earth for the dipole-dipole and the pole-dipole configurations are illustrated in Figures 22 and 23, respectively. The two-layered earth consists of a top layer of resistivity 10 ohm-m and a lower half-space of resistivity 100 ohm-m and a top-layer thickness of 100 m. A relative comparison of Figures 22 and 23 again indicates higher relative decay potentials at long off-times and all dipole separations considered for the pole-dipole configuration of the electrodes. The higher decay responses for each dipole separation for both configurations of electrodes amply illustrate the effect of the top layer of higher conductivity ($\sigma_1=10^{-1}$ mhos/m) when compared with the corresponding responses with a homogeneous half-space of the bottom-layer conductivity ($\sigma_2=10^{-2}$

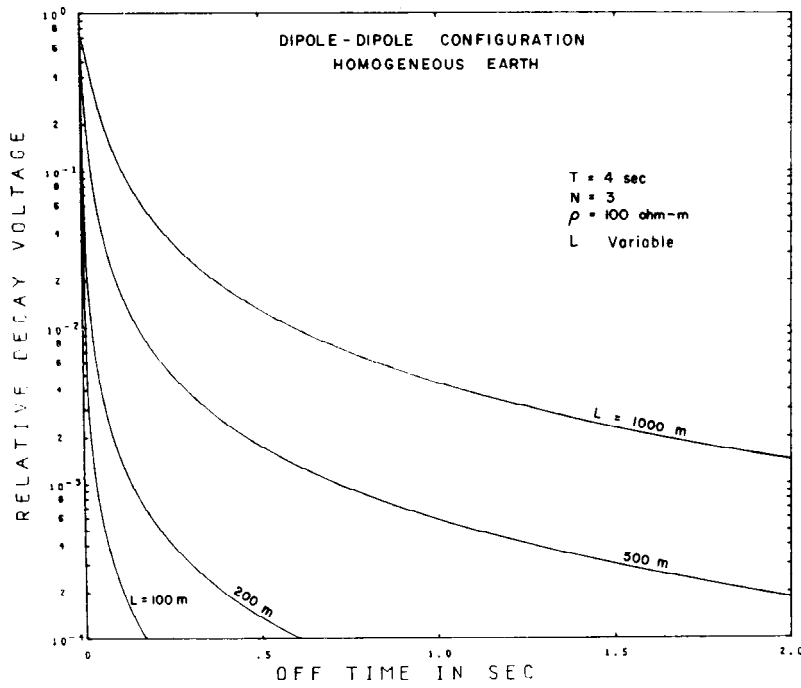


FIG. 21. Time-domain coupling response for a dipole-dipole configuration over a homogeneous earth for varying lengths of the receiver dipole.

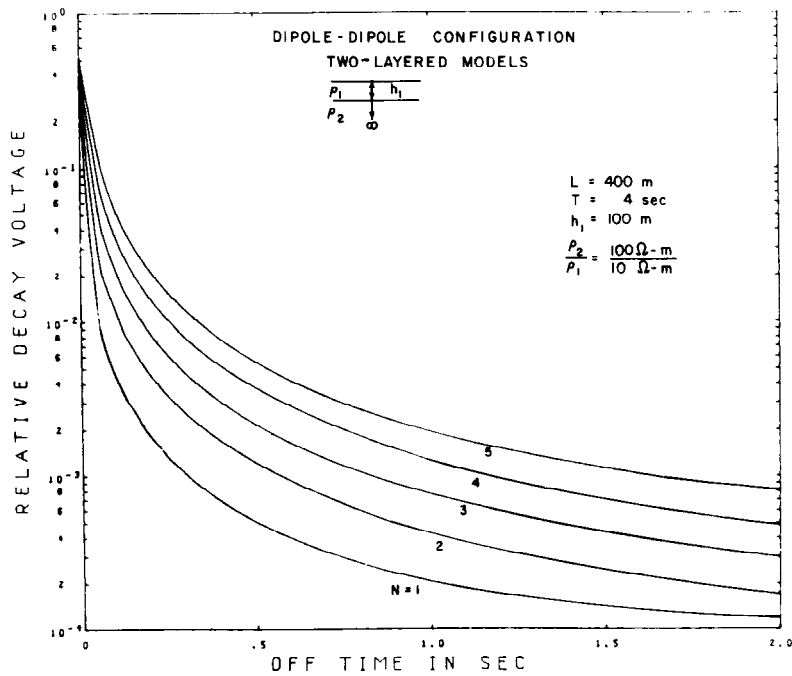


FIG. 22. Time-domain coupling response for a dipole-dipole configuration over a two-layered earth model.

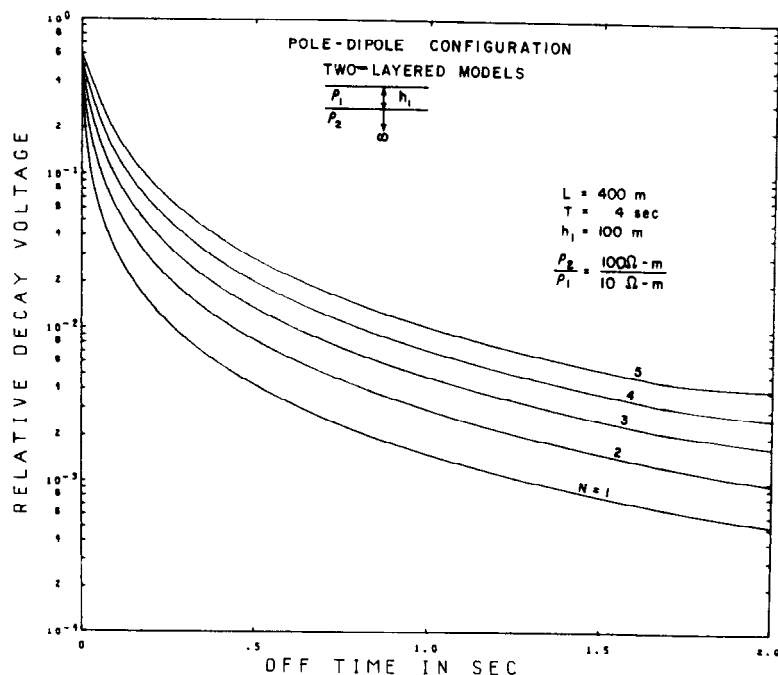


Fig. 23. Time-domain coupling response for a pole-dipole configuration over a two-layered earth model.

mhos/m). The coupling effect of the pole-dipole is considerably higher than the dipole-dipole configuration over the layered model, in that at long off-times the relative decay voltages corresponding to $N=5$ of the dipole-dipole are less than those of $N=2$ of the pole-dipole configuration of the electrodes.

Effect of conductivity contrasts.—The transient decay response over two-layered earth models with $\rho_2/\rho_1=10$ and 0.10 and homogeneous half-spaces with the resistivities of the top and the bottom layer are shown in Figure 24 for a dipole separation $N=3$. The top-layer thickness is 40 m , and the dipole-dipole electrode configuration has been assumed. A relative comparison of the responses indicates significantly larger decay voltages for a two-layered earth when resistive overburden is underlain by a more conductive half-space. The response in the case $\rho_2/\rho_1=10$ can be easily noted as distinct from the homogeneous half-space of bottom-layer resistivity, while in the case $\rho_2/\rho_1=0.1$, the layered response is influenced solely by the higher conductivity of the lower half-space.

Electromagnetic coupling over polarizable layered half-spaces

The combined results of electromagnetic coupling and normal polarization effects over a two-layered earth model are illustrated in Figures 25 and 26 for the frequency-domain and time-domain modes of operation, respectively. The two-layered model considered has a top layer of thickness 80 m and resistivity of 10 ohm-m , and it overlies a lower half-space of resistivity 100 ohm-m . A dipole length of 400 m in the dipole-dipole configuration of electrodes is used. Two different cases of polarizable half-space materials have been considered. The case I consists of a polarizable top layer with an intrinsic PFE of $15 \text{ percent per decade}$, and case II has a bottom layer with the same intrinsic normal polarizability. The combined effect of IP and coupling is evaluated by including the frequency-dependent conductivity in the generalized formulation of $Z_{ss}(\omega)$.

The electromagnetic coupling alone, when both media are nonpolarizable, exhibits the characteristic patterns for different dipole separations and off-times (for $N=4$) in frequency- and time-domain measurements. Introduction of the polar-

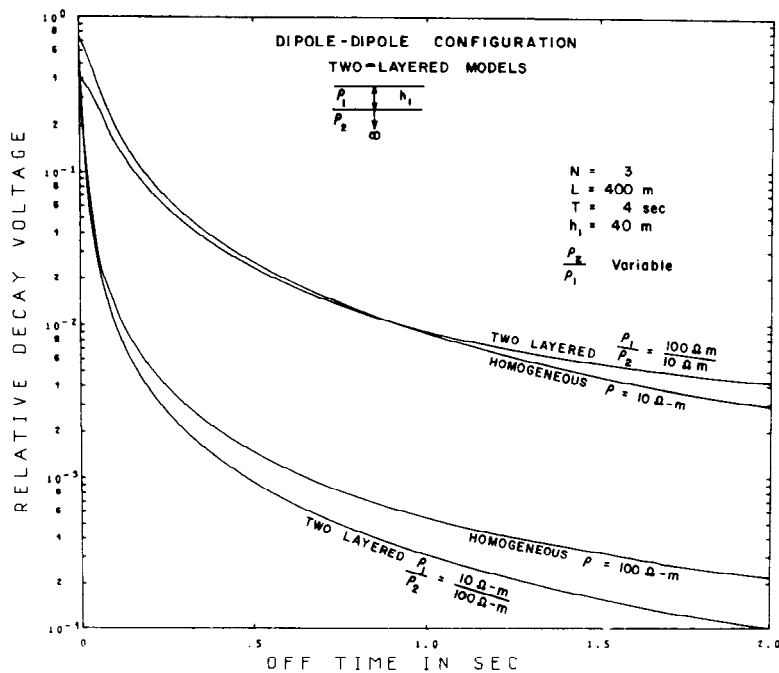


FIG. 24. Time-domain coupling response for a dipole-dipole configuration over two-layered earth models of varying conductivity contrasts.

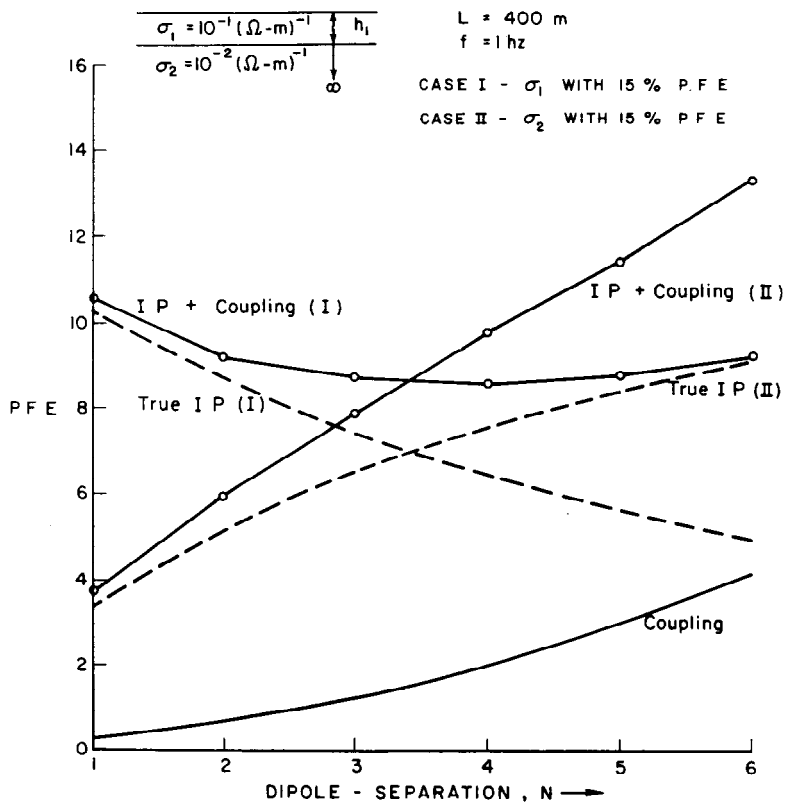


FIG. 25. Frequency-domain electromagnetic coupling responses over polarizable layered half-space models.

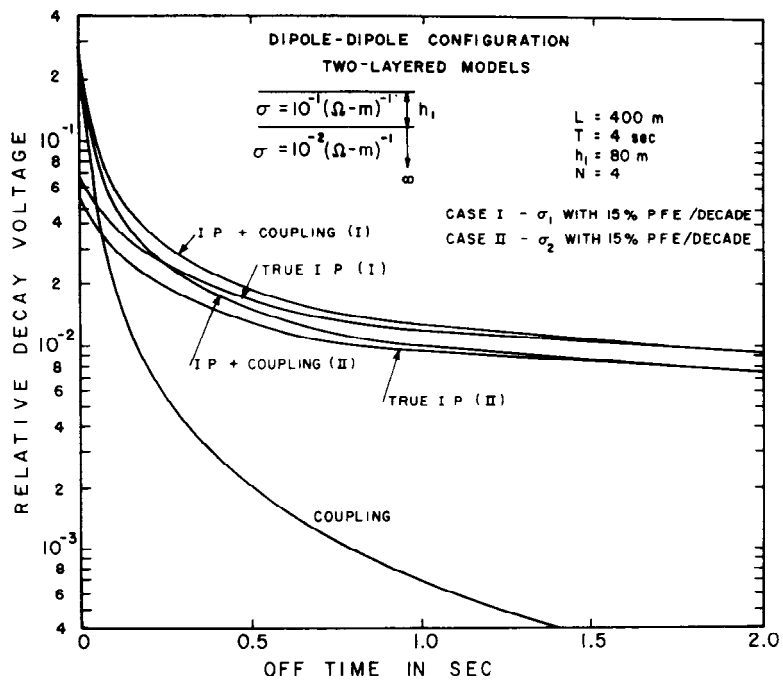


FIG. 26. Time-domain electromagnetic coupling responses over polarizable layered half-space models.

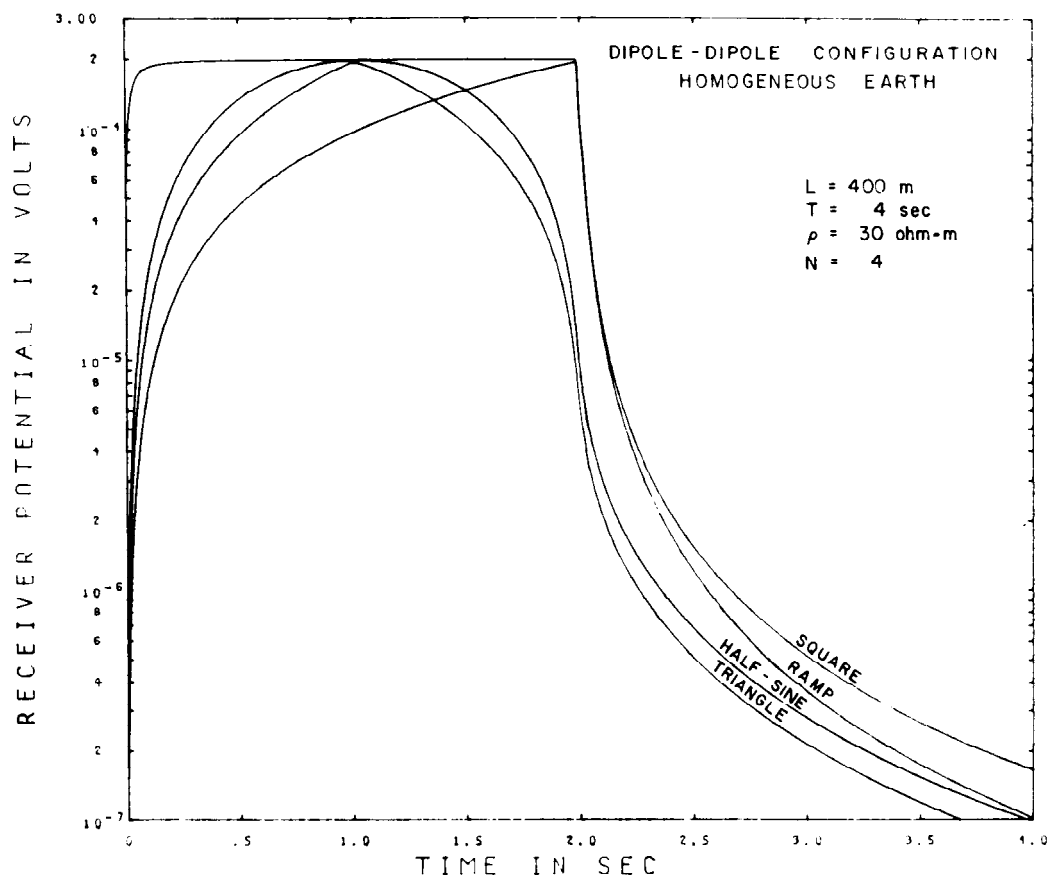


FIG. 27. Time-domain full waveform responses due to different input-current pulse shapes.

Table 1. Homogeneous half-space, $\rho = 30$ ohm-m

Input-current pulse shape	Electrode configuration	N	Pulse period (on and off) = 2.0 sec Area under curve		
			On time	Off time	Ratio
Half-sine	DP-DP	1	12.9×10^{-1}	11.4×10^{-4}	88.8×10^{-6}
		2	32.2×10^{-2}	10.7×10^{-4}	33.2×10^{-4}
		3	12.8×10^{-2}	99.4×10^{-5}	77.4×10^{-4}
		4	63.7×10^{-3}	91.8×10^{-5}	14.0×10^{-3}
	P-DP	1	19.2×10^{-1}	10.6×10^{-3}	55.4×10^{-4}
		2	62.9×10^{-2}	97.5×10^{-4}	15.4×10^{-3}
		3	30.7×10^{-2}	89.0×10^{-4}	28.9×10^{-3}
		4	17.9×10^{-2}	81.3×10^{-4}	45.3×10^{-3}
Ramp	DP-DP	1	10.0×10^{-1}	79.5×10^{-4}	79.0×10^{-4}
		2	24.8×10^{-2}	52.7×10^{-4}	21.2×10^{-3}
		3	97.6×10^{-3}	37.8×10^{-4}	38.8×10^{-3}
		4	47.8×10^{-3}	28.5×10^{-4}	59.7×10^{-3}
	P-DP	1	14.9×10^{-1}	24.7×10^{-3}	16.6×10^{-3}
		2	48.1×10^{-2}	19.5×10^{-3}	40.6×10^{-3}
		3	23.2×10^{-2}	15.9×10^{-3}	68.5×10^{-3}
		4	13.3×10^{-2}	13.2×10^{-3}	98.5×10^{-3}
Triangle	DP-DP	1	10.1×10^{-1}	82.1×10^{-5}	80.6×10^{-6}
		2	25.3×10^{-2}	77.1×10^{-5}	30.3×10^{-4}
		3	10.1×10^{-2}	71.9×10^{-5}	71.1×10^{-4}
		4	50.2×10^{-3}	66.8×10^{-5}	13.3×10^{-3}
	P-DP	1	15.1×10^{-1}	79.5×10^{-4}	52.5×10^{-4}
		2	49.5×10^{-2}	73.1×10^{-4}	14.7×10^{-3}
		3	24.2×10^{-2}	67.1×10^{-4}	27.7×10^{-3}
		4	14.1×10^{-2}	61.5×10^{-4}	43.8×10^{-3}
Square	DP-DP	1	20.2×10^{-1}	85.7×10^{-4}	42.4×10^{-4}
		2	50.1×10^{-2}	57.7×10^{-4}	11.5×10^{-3}
		3	19.8×10^{-2}	42.4×10^{-4}	21.3×10^{-3}
		4	98.2×10^{-3}	32.8×10^{-4}	33.4×10^{-3}
	P-DP	1	30.0×10^{-1}	30.4×10^{-3}	10.1×10^{-3}
		2	97.8×10^{-2}	24.6×10^{-3}	25.1×10^{-3}
		3	47.5×10^{-2}	20.5×10^{-3}	43.2×10^{-3}
		4	27.6×10^{-2}	17.5×10^{-3}	63.2×10^{-3}

izable layers, however, brings about remarkable changes in these patterns. In the case I, with the polarizable top layer, the frequency-domain response is predominantly a true IP response at smaller dipole separation, when primarily the effect of the more conductive top layer is seen. Alternately, when the lower layer is polarizable, the true IP response substantially predominates the electromagnetic coupling only at large dipole separation. In both cases considered in the frequency domain, the coupling effect is substantial, in that it represents about 50 percent of the total effect in the case I and about 30 percent in the case II at a dipole separation of $N=6$.

The time-domain transient responses ($N=4$) corresponding to the two cases considered, however, do not reflect any substantial differences in

the time IP responses. The combined effect of IP and coupling has a markedly different functional behavior at long off-times relative to that of coupling alone, when the media are nonpolarizable. For off-time measurements beyond $T_{off} > 0.6$ sec, the effect of electromagnetic coupling is practically negligible, and the transient response is almost entirely due to the intrinsic polarization effect.

Electromagnetic coupling due to different input-current pulse shapes

The receiver potentials observed over a homogeneous half-space of resistivity 30 ohm-m during the on- and off-time of input current pulses of different shape are shown in Figure 27. A dipole separation of $N=2$ for the dipole-dipole configura-

Table 2. Homogeneous half-space, $\rho = 30$ ohm-m

Input-current pulse shape	Electrode configuration	N	Pulse period (on and off) = 4.0 sec Area under curve		
			On time	Off time	Ratio
Half-sine	DP-DP	1	12.9×10^{-1}	42.1×10^{-5}	32.5×10^{-5}
		2	32.3×10^{-2}	40.3×10^{-5}	12.6×10^{-4}
		3	12.9×10^{-2}	38.4×10^{-5}	29.7×10^{-4}
		4	64.3×10^{-3}	36.4×10^{-5}	56.6×10^{-4}
	P-DP	1	19.2×10^{-1}	49.1×10^{-4}	25.4×10^{-4}
		2	63.4×10^{-2}	46.2×10^{-4}	72.8×10^{-4}
		3	31.2×10^{-2}	43.5×10^{-4}	13.9×10^{-3}
		4	18.3×10^{-2}	40.8×10^{-4}	22.2×10^{-3}
Ramp	DP-DP	1	10.1×10^{-1}	37.7×10^{-4}	37.3×10^{-4}
		2	25.0×10^{-2}	20.2×10^{-4}	10.4×10^{-3}
		3	99.4×10^{-3}	19.6×10^{-3}	19.7×10^{-3}
		4	49.1×10^{-3}	15.3×10^{-4}	31.3×10^{-3}
	P-DP	1	15.0×10^{-1}	14.3×10^{-3}	95.4×10^{-4}
		2	48.9×10^{-2}	11.6×10^{-3}	23.8×10^{-3}
		3	23.8×10^{-2}	98.2×10^{-4}	41.2×10^{-3}
		4	13.8×10^{-2}	83.9×10^{-4}	60.5×10^{-3}
Triangle	DP-DP	1	10.1×10^{-1}	29.9×10^{-5}	29.4×10^{-5}
		2	25.4×10^{-2}	28.8×10^{-5}	11.3×10^{-4}
		3	10.1×10^{-2}	27.5×10^{-5}	27.1×10^{-4}
		4	50.6×10^{-3}	26.2×10^{-5}	51.8×10^{-4}
	P-DP	1	15.1×10^{-1}	36.2×10^{-4}	23.9×10^{-4}
		2	49.9×10^{-2}	34.2×10^{-4}	68.6×10^{-4}
		3	24.5×10^{-2}	32.3×10^{-4}	13.1×10^{-3}
		4	14.4×10^{-2}	30.5×10^{-4}	21.1×10^{-3}
Square	DP-DP	1	20.2×10^{-1}	40.9×10^{-4}	20.2×10^{-4}
		2	50.4×10^{-2}	28.2×10^{-4}	55.9×10^{-4}
		3	20.0×10^{-2}	21.4×10^{-4}	10.6×10^{-3}
		4	99.7×10^{-3}	17.0×10^{-4}	17.1×10^{-3}
	P-DP	1	30.1×10^{-1}	16.9×10^{-3}	56.3×10^{-4}
		2	98.9×10^{-2}	14.0×10^{-3}	14.1×10^{-3}
		3	48.4×10^{-2}	12.0×10^{-3}	24.7×10^{-3}
		4	28.3×10^{-2}	10.4×10^{-3}	36.8×10^{-3}

tion is used with the dipole length of 400 m. The gradual build-up of the potential during on-time and the transient decay during the off-time illustrate the dispersion of the transmitted pulse as it arrives at the receiving dipole. At long off-times the absolute value of the receiver potential is the greatest for the square-current pulse and is the least when a triangle-shaped current pulse is used. The transients for the different input current pulses have different fall-off rates, since the frequency compositions of these pulses over the total time period are markedly different from each other.

The area under the receiver response curve during the on-time and the off-time segments of the pulse for the dipole-dipole and the pole-dipole

configurations have been shown in Tables 1 and 2 for dipole separations $N = 1, 2, 3, 4$. Two different periods of the pulses, consisting of 2 and 4 sec, are considered. The ratio of the off-time area to the on-time area is a diagnostic measure of the net electromagnetic coupling response. A comparison of these ratios for both the dipole-dipole and the pole-dipole configurations indicates a minimum coupling effect for $T = 2$ and 4 sec when a half-sine or triangle-shaped input-current excitation function is used.

CONCLUSION

A completely general solution of electromagnetic fields over a multilayered half-space is formulated for grounded dipoles of finite length.

Electromagnetic coupling responses are derived therefrom for induced-polarization measurements made in both frequency- and time-domain modes. The effects of layering as distinct from homogeneous half-space responses are clearly shown for different electrode configurations, layer geometry, and electrical parameters. While coupling responses in frequency- and time-domain measurements for a uniform half-space are of generally similar pattern, the inadequacy of effecting a coupling correction in a layered situation using a homogeneous half-space model is demonstrated.

In time-domain measurements, a lumped effect of a number of frequencies is observed, and over a polarizable half-space long off-time transient responses are generally noted to be free of the coupling effect. The frequency-domain measurements, however, show the coupling effects to be a substantial fraction of the overall response observed over polarizable half-spaces or long dipole separations. The comparison of the transient responses of input current waveforms of various shapes and time periods indicates a minimum coupling effect for a half-sine or triangle-shaped current excitation function.

ACKNOWLEDGMENT

This work was partially funded by The Anacosta Company.

REFERENCES

- Bhattacharyya, B. K., 1957, Propagation of an electric pulse through a homogeneous and isotropic medium: *Geophysics*, v. 22, p. 905.
- 1964, Electromagnetic fields of a small loop antenna on the surface of a polarizable medium: *Geophysics*, v. 29, p. 814.
- Cooley, J. M., and Tukey, J. M., 1965, An algorithm for the machine calculation of complex Fourier series: *Math. of Comput.*, v. 19, p. 297.
- Dey, A., and Ward, S. H., 1970, Inductive sounding of a layered earth with a horizontal magnetic dipole: *Geophysics*, v. 35, p. 660.
- Dey, A., Morrison, H. F., and Ward, S. H., 1970, Electric fields from a horizontal electric dipole situated above a layered lunar half-space: Final Rep. NASA Contract NAS2-5078, Space Sciences Laboratory Series 11, Issue 21.
- Foster, R. N., 1933, Mutual impedance of grounded wires lying on or above the surface of the earth: *Bell System Tech. J.*, v. 12.
- Hohmann, G. W., 1970, Electromagnetic coupling between grounded wires at the surface of a two-layer earth: personal communication.
- Millett, F. B., 1967, Electromagnetic coupling of collinear dipoles on a uniform half-space, in *Mining geophysics*, v. 2: Tulsa, SEG.
- Morrison, H. F., Phillips, R. J., and O'Brien, D.P., 1969, Quantitative interpretation of transient electromagnetic fields over a layered half-space: *Geophys. Prosp.*, v. 17, p. 82.
- Riordan, J., and Sunde, E. D., 1933, Mutual impedance of grounded wires for stratified two-layer earth: *Bell System Tech. J.*, v. 12.
- Sunde, E. D., 1968, *Earth conduction effects in transmission systems*: New York, Dover.
- Vanyan, L. L., 1967, *Electromagnetic depth soundings: selected and translated by George V. Keller*, Consultants Bureau, New York.
- Wait, J. R., 1951, The magnetic dipole over the horizontally stratified earth: *Can. J. of Physics*, v. 29, p. 577.
- 1960, Propagation of electromagnetic pulses in a homogeneous conducting earth: *Appl. Sci. Res.*, Section B, v. 9, p. 213.
- 1966, Fields of a horizontal dipole over a stratified anisotropic half-space: *IEEE transactions on Antenna and Propagation*, AP.14, p. 790.